Optimal Offering Strategy of Virtual Power Plant with Hybrid Renewable Ocean Energy Portfolio

Siyuan Guo, *Student Member*, *IEEE*, Bin Zhou, *Senior Member*, *IEEE*, *Member*, *CSEE*, Ka Wing Chan, *Member*, *IEEE*, Siqi Bu, *Senior Member*, *IEEE*, Canbing Li, *Senior Member*, *IEEE*, Nian Liu, *Member*, *IEEE*, and Cong Zhang, *Member*, *IEEE*

***Abstract*—This paper proposes a hybrid ocean energy system to form a virtual power plant (VPP) for participating in electricity markets in order to promote the renewable ocean energy utilization and accommodation. In the proposed system, solar thermal energy is integrated with the closed-cycle ocean thermal energy conversion (OTEC) to boost the temperature differences between the surface and deep seawater for efficiency and flexibility improvements, and the thermodynamic effects of seawater mass flow rates on the output of solar-boosted OTEC (SOTEC) are exploited for deploying SOTEC as a renewable dispatchable unit. An optimal tidal-storage operation model is also developed to make use of subsea pumped storage (SPS) with hydrostatic pressures at ocean depths for mitigating the intermittent tidal range energy in order to make the arbitrage in the electricity market. Furthermore, a two-stage coordinated scheduling strategy is presented to optimally control seawater mass flow rates of SOTEC and hydraulic reversible pump-turbines of SPS for enhancing the daily VPP profit. Comparative studies have been investigated to confirm the superiority of the developed methodology in various renewable ocean energy and electricity market price scenarios.**

***Index Terms*—Ocean thermal energy conversion, rolling optimization, subsea pumped storage system, tidal power generation, virtual power plant.**

I. Introduction

A. Motivation

OCEAN energy has theoretical resource potential to meet present and projected global electricity demand well into the future [1]. Compared to other types of renewable energy, ocean energy resources have numerous advantages including consistency, predictability, abundance and lower environmental impacts [2]. However, renewable ocean energy sources only account for a minuscule part of the global energy supply despite the ocean encompassing about 71% of the earth's surface area with vast potential energy to exploit [3]. The total cumulative capacity of the offshore wind power plant (OWPP) in China only accounts for 0.7% of national technical potential for offshore wind energy utilization [4]. With the penetration of renewable ocean energy into the electric power grid extensively increasing, the inherent fluctuating and volatile characteristics of renewable ocean energy have brought challenges to the stability and security of smart grid [5]–[7].

Due to the inherent seasonality, instability and dispersion of renewable ocean energy resources, their harvesting and utilization exhibit a low degree of efficiency and grid availability [1]. The low efficiency of a single ocean energy resource, such as ocean thermal energy conversion (OTEC) [8], [9], seriously hinders the commercialization and advancement of ocean energy. The hybridization of multiple ocean energy technologies can make full use of their energy complementarities, and thus provide a promising approach to improve system stability and energy efficiency. This paper strives to investigate the integration of various renewable ocean energy sources, such as OWPP, tidal power plant (TPP) and OTEC, to form a hybrid energy virtual power plant (VPP) for promoting renewable ocean energy harvesting and accommodation [10].

B. Literature Review

So far, a large number of existing research studies in [1]–[5] have been devoted to investigating the modeling and operation of various ocean energy resources. The layout architectures of offshore wind farms were designed and optimized in [11], [12] to ensure their stable and efficient operation. The thermodynamic modeling and parametric optimization techniques for different hygro-thermal cycles were investigated in [13]–[15] to improve the energy conversion efficiency of OTEC. The sophisticated hydrodynamic modeling of TPP was studied in [16], [17] to optimize the operational mode in response to time-varying tidal ranges. Despite the fact that operational obstacles of a single ocean energy technology have been settled, the development of renewable ocean energy sources is still not being developed due to their low return on investment and inherent fluctuations [1]–[3]. In recent years, various ocean

Manuscript received November 29, 2020; revised March 31, 2021; accepted June 15, 2021. Date of online publication September 10, 2021; date of current version November 17, 2022. This work was jointly supported by the Sino-US International Science and Technology Cooperation Project (No. 2019YFE0114700), the National Natural Science Foundation of China (No. 51877072) and the State Key Laboratory of Alternate Electrical Power System with Renewable Energy Sources (No. LAPS20005).

S. Y. Guo, B. Zhou (corresponding author, email: binzhou@hnu.edu.cn; ORCID: https://orcid.org/0000-0002-1376-4531) and C. Zhang are with the College of Electrical and Information Engineering, Hunan University, Changsha 410082, China.

K. W. Chan and S. Q. Bu are with the Department of Electrical Engineering, The Hong Kong Polytechnic University, Hong Kong, China.

C. B. Li is with the School of Electronic Information and Electrical Engineering, Shanghai Jiao Tong University, Shanghai 200240, China.

N. Liu is with the State Key Laboratory of Alternate Electrical Power System with Renewable Energy Sources, North China Electric Power University, Beijing 102206, China.

DOI: 10.17775/CSEEJPES.2020.06420

energy resources, such as OWPP, OTEC and solar energy, have been integrated in [18], [19] to utilize the flexibility provided by their mutual interconnections for reliable and renewable power supplies.

The VPP can be employed as an aggregator to incorporate various renewable ocean energy sources and energy storage systems (ESSs) for their flexibility enhancement, and thus can be pooled for participating in the electricity market to increase the VPP profitability [20], [21]. Most of the existing literatures focused on optimizing scheduling, offering and bidding strategies as well as the energy portfolio of the VPP in electricity markets [22]–[28]. Stochastic programming models were extensively formulated in [23], [24] to characterize the uncertain renewable generation outputs and market prices by a set of stochastic scenarios for optimizing the scheduling of energy mix resources. Further studies were investigated in [25], [26] to develop robust bidding models of the VPP by formulating the confidence bounds to reduce the computational burden and mitigate commercial risks resulting from volatile market prices. Various ESS technologies, such as the pumped hydro energy storage [22], battery energy storage [23], [24], and electric vehicles [27]–[29], have been integrated into the VPP to mitigate inherent fluctuations from renewable energy. However, the studies on the optimal offering strategy of the VPP to facilitate the utilization and accommodation of renewable ocean energy resources are still not involved.

C. Contribution

In this study, a hybrid renewable ocean energy system is formed as a VPP for participating in electricity markets in order to promote ocean energy harvesting and accommodation. A two-stage coordinated scheduling strategy is also presented for optimally controlling seawater mass flow rates of solar-boosted OTEC (SOTEC) and hydraulic reversible pump-turbines of the subsea pumped storage (SPS) to enhance the thermal efficiency of SOTEC and total daily profit under uncertainties of renewable ocean energy and electricity market prices. The contributions of this paper are summarized as follows:

1) Solar thermal energy is integrated to boost the temperature of surface warm seawater so as to enhance the energy extraction from the closed Rankine cycle for efficiency and flexibility improvements, and thermodynamic models of the evaporator and working fluid pump are formulated to investigate the effects of the coordination between warm and cold seawater mass flow rates on the output of SOTEC.

2) A coordinated tidal-storage operation model is proposed to utilize SPS with the hydrostatic pressure at ocean depth to mitigate the intermittent tidal range energy, and the TPP output can be complemented with SPS by pumping seawater out of an undersea reservoir and later allowing it to flow back in to make the arbitrage in the electricity market.

II. Problem Formulation

A. Overview

In this paper, the VPP is composed of OWPP, TPP with SPS and SOTEC. The OWPP and TPP outputs are fluctuating due to the inherent intermittency and volatile characteristics of wind and tide. On the contrary, SOTEC and SPS are both dispatchable. The diurnal fluctuations of volatile and intermittent renewable ocean energy resources can be offset by the time complementarities between offshore wind, solar and tidal resources. As the performances of OTEC are severely limited by its low efficiency, solar energy is integrated into ocean thermal energy for flexibility and efficiency enhancements. Moreover, utilizing the hydrostatic pressure at ocean depth, the water level in the tidal reservoir is coupled with tidal range by SPS to mitigate the intermittent tidal energy.

These distributed renewable ocean energy installations are corporately managed by a central control entity. With the dispatchable SOTEC and SPS, VPP can flexibly participate in the electricity market to boost daily profit. Moreover, the day-ahead and balancing market are both taken into consideration for flexible energy trading. In the day-ahead market, the VPP submits the offering curve for the day-ahead scheduling of electricity market transactions. In the balancing market, the VPP can sell or purchase electricity for balancing differences between committed values and specific realizations of renewable ocean energy.

B. OTEC Model With Solar Enhancement

The OTEC utilizes the thermal gradient of the ocean to generate electricity which creates steam through the heat source of surface warm seawater and recondenses the steam through the deep cold seawater [10]. As shown in Fig. 1, the working fluid with a low boiling point, such as ammonia, is heated by warm seawater to obtain the vapor in a closed-cycle OTEC. Then the vapor turns the turbine to drive a generator. With the vapor condensed by the cold seawater, the working fluid ultimately is cycled back by the working fluid pump. Therefore, the OTEC output can be controlled by coordinating the seawater mass flow rates so as to adjust the enthalpy of the working fluid [5], [30]. However, on account of the small temperature differences between surface warm seawater and deep cold seawater, the efficiency of conventional OTEC is only 3.5% to 4% [8].

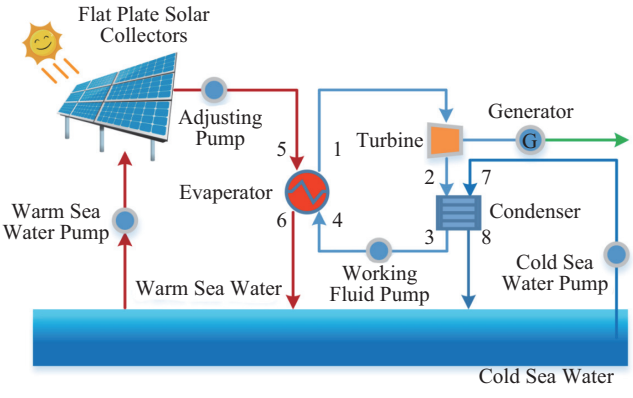

Fig. 1. Schematic diagram of SOTEC.

In this study, solar collectors are combined with OTEC to boost the heat resource for the efficiency and flexibility enhancement of OTEC. Moreover, the thermodynamic effects

of the coordination between warm and cold seawater mass flow rates on SOTEC output are investigated to deploy it as the dispatchable unit. Fig. 2 shows the T-s diagram of OTEC [9]. Here, T_{CSI} and T_{CSO} are temperatures of the inlet and outlet cold seawater, T_{WSI} and T_{WSO} are temperatures of the inlet and outlet warm seawater, T_{C} and T_{E} are the condensing temperature and evaporating temperature, T_{SCO} is the outlet temperature of the warm seawater flowing through solar collectors.

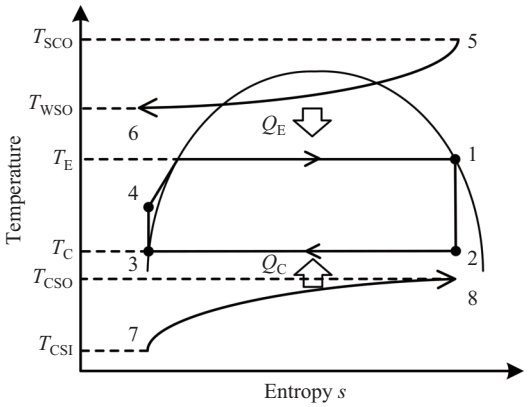

Fig. 2. T-s diagram of closed OTEC.

The output power of SOTEC P_{e} is calculated as follows,

$$P_{\mathrm{e}} = m_{\mathrm{WF}}\eta_{\mathrm{tur}}\eta_{\mathrm{gen}}(h_1 - h_2) \tag{1}$$

where m_{WF} is the mass flow rate of the working fluid. h_1 and h_2 are specific enthalpies of the working fluid at the turbine inlet and outlet. η_{tur} is the efficiency of the turbine and η_{gen} is the efficiency of the generator. The values of all enthalpies are calculated by the software REFPROP 9.0 [31]. The consumptions of the cold seawater pump P_{CS}, warm seawater pump P_{WS}, working fluid pump P_{WF} and adjusting pump P_{AD} are calculated as follows,

$$P_{\mathrm{CS}} = m_{\mathrm{CS}}\Delta H_{\mathrm{CS}}g/\eta_{\mathrm{CSP}} \tag{2}$$

$$P_{\mathrm{WS}} = m_{\mathrm{WS}}\Delta H_{\mathrm{WS}}g/\eta_{\mathrm{WSP}} \tag{3}$$

$$P_{\mathrm{AD}} = m_{\mathrm{AD}}\Delta H_{\mathrm{AD}}g/\eta_{\mathrm{ADP}} \tag{4}$$

$$P_{\mathrm{WF}} = m_{\mathrm{WF}}\Delta H_{\mathrm{WF}}g/\eta_{\mathrm{WFP}} = m_{\mathrm{WF}}(h_4 - h_3) \tag{5}$$

where m_{CS} and m_{WS} are mass flow rates of cold seawater and warm seawater; h_3 and h_4 are specific enthalpies of the working fluid at the working fluid pump inlet and outlet. η_{CSP}, η_{WSP}, η_{ADP} and η_{WFP} are efficiencies of the cold seawater pump, warm seawater pump, adjusting pump and working fluid pump, respectively. ΔH_{CS}, ΔH_{WS}, ΔH_{AD}, and ΔH_{WF} are all the frictional head losses and they are calculated [14] as follows,

$$\Delta H = fv^2L/2Dg \tag{6}$$

$$v = 4m/\pi D^2\rho \tag{7}$$

where f is the friction factor of the pipe or fitting; D is the diameter of the pipe; L is the pipe length; V, ρ and m are the velocity, density and mass flow rate of the seawater or working fluid, respectively.

Based on the conservation of energy in the heat-exchanging model of the evaporator and condenser, the energy balance can be written [32], [33] as follows,

$$Q_{\mathrm{E}} = m_{\mathrm{WF}}(h_1 - h_4) = m_{\mathrm{AD}}C_{\mathrm{P}}(T_{\mathrm{SCO}} - T_{\mathrm{WSO}})\eta_{\mathrm{E}} \tag{8}$$

$$Q_{\mathrm{C}} = m_{\mathrm{WF}}(h_2 - h_3) = m_{\mathrm{CS}}C_{\mathrm{P}}(T_{\mathrm{CSO}} - T_{\mathrm{CSI}})\eta_{\mathrm{C}} \tag{9}$$

where Q_{E} and Q_{C} are heat flow rates of the condenser and evaporator, respectively; C_{p} is the heat capacity of the seawater; η_{E} and η_{C} are efficiencies of the evaporator and condenser, respectively. The heat transfer coefficient K is calculated as follows [34],

$$K = \left(\frac{1}{\alpha_{\mathrm{S}}} + R_{\mathrm{S}} + \frac{1}{\alpha_{\mathrm{WF}}} + R_{\mathrm{WF}} + \frac{\delta_{\mathrm{P}}}{\lambda_{\mathrm{P}}}\right) \tag{10}$$

where α_{S} and α_{WF} are the surface heat transfer coefficients on the seawater and working fluid sides, R_{S} and R_{WF} are the fouling resistances on the seawater and working fluid sides, δ_{P} and λ_{P} are the heat transfer plate thickness and thermal conductivity. The heat transfer areas of the evaporator A_{E} and condenser A_{C} can be calculated as follows,

$$A_{\mathrm{E}} = \frac{Q_{\mathrm{E}}}{K_{\mathrm{E}}\Delta T_{\mathrm{E}}} \tag{11}$$

$$A_{\mathrm{C}} = \frac{Q_{\mathrm{C}}}{K_{\mathrm{C}}\Delta T_{\mathrm{C}}} \tag{12}$$

where ΔT_{E} and ΔT_{C} are the logarithmic mean temperature differences in evaporation and condensation sections. The logarithmic mean temperature difference can be calculated by the following formula,

$$\Delta T = \frac{(T_{\mathrm{S,in}} - T_{\mathrm{WF,in}}) - (T_{\mathrm{S,\,out}} - T_{\mathrm{WF,out}})}{\ln\left(\frac{T_{\mathrm{S,in}} - T_{\mathrm{WF,in}}}{T_{\mathrm{S,\,out}} - T_{\mathrm{WF,out}}}\right)} \tag{13}$$

where $T_{\mathrm{S,in}}$ is the temperature of the seawater flowing in the evaporator or condenser; $T_{S,\mathrm{out}}$ is the temperature of the seawater flowing out of the evaporator or condenser; $T_{\mathrm{WF,in}}$ is the temperature of the working fluid flowing in the evaporator or condenser; $T_{\mathrm{WF,out}}$ is the temperature of the working fluid flowing out of the evaporator or condenser. Based on (1), (8) and (9), the thermodynamic connection between seawater mass flow rates and SOTEC output can be expressed as follows,

$$P_{\mathrm{e}} = \frac{m_{\mathrm{AD}}(h_1 - h_2)(T_{\mathrm{SCO}} - T_{\mathrm{WSO}})\eta_{\mathrm{tur}}\eta_{\mathrm{gen}}C_{\mathrm{p}}}{h_1 - h_4} \tag{14}$$

$$P_{\mathrm{e}} = \frac{m_{\mathrm{CS}}(h_1 - h_2)(T_{\mathrm{CSO}} - T_{\mathrm{CSI}})\eta_{\mathrm{tur}}\eta_{\mathrm{gen}}C_{\mathrm{p}}}{h_2 - h_3} \tag{15}$$

Therefore, SOTEC output can be controlled by the coordination between warm and cold seawater mass flow rates.

The net power P_{N} of SOTEC and the consumptions of pumps can be calculated as follows,

$$P_{\mathrm{N}} = P_{\mathrm{e}} - (P_{\mathrm{WS}} + P_{\mathrm{CS}} + P_{\mathrm{AD}} + P_{\mathrm{WF}}) \tag{16}$$

$$P_{\mathrm{CS}} = \frac{8P_{\mathrm{e}}^3(h_2 - h_3)^3L_{\mathrm{CS}}f}{(h_1 - h_2)^3\eta_{\mathrm{tur}}^3\eta_{\mathrm{gen}}^3(T_{\mathrm{CSO}} - T_{\mathrm{CSI}})^3 D_{\mathrm{CS}}^5\rho^2\pi^2\eta_{\mathrm{CSP}}\eta_{\mathrm{C}}^3C_{\mathrm{p}}^3} \tag{17}$$

$$P_{\mathrm{AD}} = \frac{8P_{\mathrm{e}}^3(h_1 - h_4)^3L_{\mathrm{AD}}f}{(h_1 - h_2)^3\eta_{\mathrm{tur}}^3\eta_{\mathrm{gen}}^3(T_{\mathrm{SCO}} - T_{\mathrm{CSI}})^3 D_{\mathrm{AD}}^5\rho^2\pi^2\eta_{\mathrm{ADP}}\eta_{\mathrm{E}}^3C_{\mathrm{p}}^3} \tag{18}$$

$$P_{\mathrm{WS}} = 8m_{\mathrm{WS}}^3 L_{\mathrm{WS}} f / D_{\mathrm{WS}}^5 \rho^2 \pi^2 \eta_{\mathrm{WSP}} \tag{19}$$

$$P_{\mathrm{WF}} = P_{\mathrm{e}}(h_4 - h_3)/\eta_{\mathrm{tur}}\eta_{\mathrm{gen}}(h_1 - h_2) \tag{20}$$

The flat plate solar collectors are utilized to promote the flexibility and efficiency of SOTEC. The thermal energy Q_{u} provided by the working fluid can be calculated as follows,

$$Q_{\mathrm{u}} = m_{\mathrm{WS}} C_{\mathrm{p}} (T_{\mathrm{SCO}} - T_{\mathrm{WSI}}) \tag{21}$$

The Hottel–Whillier equation [35] for thermal energy The Hottel–Whillier equation [35] for thermal energy Q_{u} of a solar thermal collector system is,

$$Q_{\mathrm{u}} = A_{\mathrm{sc}} F_{\mathrm{R}} [S - U_{\mathrm{L}}(T_{\mathrm{WSI}} - T_{\mathrm{a}})] \tag{22}$$

where A_{sc} is the area of the flat solar collectors; S is the radiation absorbed flux by unit area of the absorber plate; U_{L} is the overall loss coefficient; T_{a} is the ambient temperature; F_{R} is the heat removal factor and is defined as follows,

$$F_{\mathrm{R}} = \frac{m_{\mathrm{WS}} C_{\mathrm{p}}}{A_{\mathrm{sc}} U_{\mathrm{L}}} \left[1 - \exp\left(-\frac{A_{\mathrm{sc}} U_{\mathrm{L}} F'}{m_{\mathrm{WS}} C_{\mathrm{p}}}\right)\right] \tag{23}$$

where F' is the collector efficiency factor.

C. Tidal-stpply Electricity Reliably and Sorage Operation Model With SPS

Despite the fluctuation of tidal energy, it is highly predictable because of its obvious daily, weekly and annual cycles. Nevertheless, tidal power generation is close to zero for about 4 hours during every tide. Therefore, there is profit potential to couple tidal generation with ESS. The intermittent output can be optimized by the utilization of ESS which stores excess tidal power when demand is low and releases energy at times of high demand to make the arbitrage.

The TPP consists of a dam built across a bay, with channels built over the dam containing several lines of in-stream turbines as shown in Fig. 3. In this way, with the barrage built across the bay, tides are blocked in the coastal basin. When turbine gates are opened, the seawater is forced to flow through narrow channels for intensifying tidal currents. The TPP optimizes the amount of harvestable energy under the model of ebb generation. When the flood tide occurs, the seawater flows into the basin through the sluices. During the ebb tide, the seawater level outside the basin drastically decreases. With the turbine gates opened, seawater flows out of the tidal reservoir driving the turbines to generate electricity. Therefore, flood tide is related to basin filling and ebb tide corresponds to basin emptying.

In this paper, the TPP is integrated with SPS to surmount the intermittent and improve the flexibility of the TPP. The SPS comprises a thin-shelled concrete ellipsoid with a chamber that is anchored to the sea floor and performs as a reservoir, valves, hydraulic reversible pump-turbines, and generators [36] as shown in Fig. 4. The subsea reservoir is located at 30 m deep under the sea and the average hydraulic pressure is 302.82 kPa [37]. With the hydrostatic pressure at ocean depth, SPS can store or release energy. The pumped hydro units pump the seawater out of the reservoir through valves to store the excessive energy, and the valves in the evacuated reservoir are opened when the SPS releases energy to let the seawater

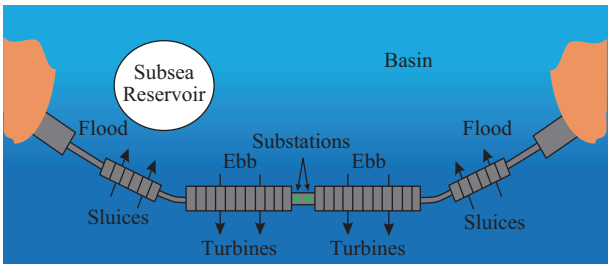

Fig. 3. Sketched vertical view of TPP.

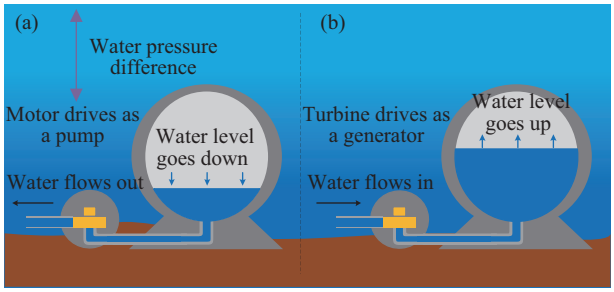

Fig. 4. Internal view of subsea pumped storage during (a) charging and (b) discharging.

flow in the tidal reservoir turning the turbine and generating electricity. Therefore, the TPP coupled with SPS could offer a synergistic method to supply electricity reliably and steadily,

$$St_{\mathrm{t}} = St_{t-1} + P_{\mathrm{pu},t} Ef_{\mathrm{pu}} - P_{\mathrm{tu},t}/Ef_{\mathrm{gen}} \tag{24}$$

where St_{t} and St_{t-1} are the energy state of SPS at hour t and $t-1$, respectively; $P_{\mathrm{pu},t}$ and $P_{\mathrm{tu},t}$ are the power of the pump and turbine in the SPS at hour t, respectively; Ef_{pu} and Ef_{gen} are the efficiencies of the pump and turbine, respectively. Maximum energy state of SPS occurs when the subsea reservoir is empty and the inside volume remains at or below atmospheric pressure. Therefore, the total capacity of SPS is related to the located ocean depth and the inner volume of the subsea reservoir. The discharge process ends when the subsea reservoir is full of seawater.

The TPP operates under the mode of ebb generation in which the turbine only works when the ebb tide is in the same flow direction [17]. When the ebb tide happens, the operations of TPP are divided into four steps including filling, holding, generating and holding as shown in Fig. 5:

1) The basin upstream of the barrage is filled with seawater flowing through the sluices when the high tide occurs. Then the sluice gates would be closed until the tidal reservoir level is equal to the sea level (filling section from A to B).

2) The sluice and turbine gates are both kept closed until the sea level decreases to form an adequate water head. Here H_{st} is named as the starting water head (holding section from B to C).

3) The turbine gates are opened so that the seawater flows out of the tidal reservoir driving turbines to generate electricity until the water head is not high enough to drive turbines. Here the low water head is defined as the minimum water head H_{min} (generating section from C to D).

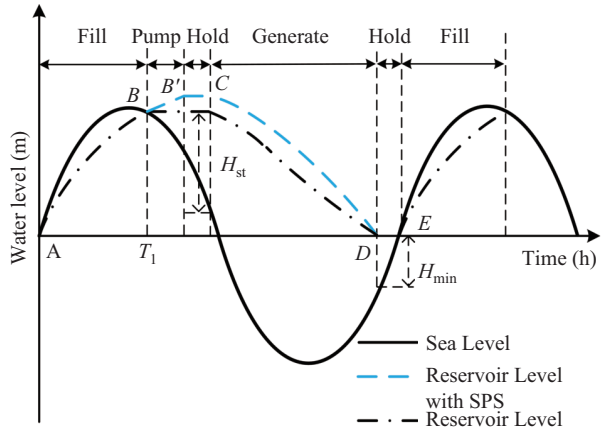

Fig. 5. Sketched water level of tidal reservoir.

4) Because of the low water head, the turbine and sluice gates would be closed again until the sea level is higher than the reservoir level (holding section from D to E).

When the TPP is integrated with SPS, the seawater level of the tidal reservoir changes as shown in Fig. 5. Assuming that there is a redundant energy need to be stored at time T_1, obviously the water head of the tidal reservoir with SPS is higher due to the pumped seawater from the subsea reservoir, which contributes to the greater output power. Moreover, the operator of the TPP can also make the arbitrage by storing excessive or off-peak energy and selling electricity at the peak market price. The specific quantity of the stored or released energy is related to the power price differential and strategic market decisions.

III. Modeling and Methodology

A. Day-ahead Offering Strategy

The offering strategy of the VPP takes into account both the day-ahead market and balancing market, which provides the operator of the VPP with flexible energy trading. In the day-ahead market, the VPP is regarded as a price taker and submits offers to the day-ahead market several hours before the operation hour. With inherent uncertainties of offshore wind, tidal and solar power, the operator has to sell or purchase electricity in the balancing market for settling differences between committed values and specific realizations of renewable ocean energy. Based on the European power market, transactions in the balancing market adopt the dual pricing strategy [22], [23].

In this paper, a two-stage coordinated scheduling strategy combined with rolling horizon optimization is utilized for optimally controlling the seawater mass flow rates of SOTEC and hydraulic reversible pump-turbines of SPS to promote the thermal efficiency of SOTEC and total daily profit [38], [39]. In the first stage, the offering curve should be provided by the operator in the day-ahead market. It is worth noting that there is no scheduling plan made until the output of renewable ocean energy becomes known. As the proposed VPP is a 100% renewable ocean energy system without fossil fuel cost, the developed profit-maximization scheduling model is devoted to obtaining the optimal offering curve in the day-ahead market and trading strategy in the balancing market, and controlling various dispatchable devices for the optimal coordination among adoptive renewable ocean energy. The goal of the optimal scheduling model is to maximize the expected profit of the VPP which contains the amount of electricity purchased or sold in the day-ahead market $G_{s,t}$, electricity sold at a low price in the balancing market $g^{\mathrm{d}}_{s,t}$, electricity bought at a high price in the balancing market $g^{\mathrm{up}}_{s,t}$, star-up cost of SOTEC F_{o}, and star-up cost of the charging units F_{tur} and discharging units F_{pu} in SPS, as follows,

$$\max \sum_{t=1}^{N_{\mathrm{H}}}\sum_{s=1}^{N_{\mathrm{R}}}\pi_{\mathrm{s}}\left[\lambda_{s,t}(G_{s,t}+g^{\mathrm{d}}_{s,t}\cdot\varphi_{\mathrm{d}}-g^{\mathrm{up}}_{s,t}\varphi_{\mathrm{up}}) -y_{s,t}F_{\mathrm{o}}-z_{s,t}F_{\mathrm{tu}}-l_{s,t}F_{\mathrm{pu}}\right] \quad (25)$$

where π_{s} is the probability of the sth scenario; $\lambda_{s,t}$ is the day-ahead market price in the scenario s and time t; N_{H} is the number of time periods; N_{R} is the number of scenarios for the day-ahead scheduling. φ_{d} and φ_{up} are the down-regulation and up-regulation price ratios, respectively; $y_{s,t}$ is the binary variable that is equal to 1 if SOTEC starts up at time t, and 0 otherwise; $z_{s,t}$ and $l_{s,t}$ are binary variables whose values are 1 if the turbine and pump of SPS start up at time t, respectively, and 0 otherwise. The system constraints are depicted as follows and the following constraints hold for any s in scenarios N_{R}.

1) SOTEC Constraints

The equality constraints of the pump consumptions are based on the thermodynamic model in Section 2. Moreover, the SOTEC has to enforce the minimum-down and minimum-up time constraints due to the physical properties and operational requirements of the units,

$$x_{s,t},y_{s,t}\in\{0,1\}\quad\forall t \quad (26)$$

$$x_{s,t}-x_{s,t-1}\le y_{s,t}\quad\forall t \quad (27)$$

$$P_{\mathrm{e,min}}x_{s,t}\le P_{\mathrm{e},s,t}\le P_{\mathrm{e,max}}x_{s,t}\quad\forall t \quad (28)$$

$$m_{\mathrm{CS},s,t}=\frac{P_{\mathrm{e},s,t}(h_{2,s}-h_{3,s})}{(h_{1,s}-h_{2,s})\eta_{\mathrm{gen}}\eta_{\mathrm{tu}}C_{\mathrm{P}}(T_{\mathrm{CSO}}-T_{\mathrm{CSI}})}\quad\forall t \quad (29)$$

$$m_{\mathrm{AD},s,t}=\frac{P_{\mathrm{e},s,t}(h_{1,s}-h_{4,s})}{(h_{1,s}-h_{2,s})\eta_{\mathrm{gen}}\eta_{\mathrm{tu}}C_{\mathrm{P}}(T_{\mathrm{SCO},s}-T_{\mathrm{WSO}})}\quad\forall t \quad (30)$$

$$m_{\mathrm{WF},s,t}=P_{\mathrm{e},s,t}/(h_{1,s}-h_{2,s})\eta_{\mathrm{gen}}\eta_{\mathrm{tu}}\quad\forall t \quad (31)$$

$$P_{\mathrm{WS},s,t}=8(m_{\mathrm{WS},s,t})^3fL_{\mathrm{WS}}/D^5_{\mathrm{WS}}\rho^2\eta_{\mathrm{WSP}}\quad\forall t \quad (32)$$

$$P_{\mathrm{CS},s,t}=8(m_{\mathrm{CS},s,t})^3fL_{\mathrm{CS}}/D^5_{\mathrm{CS}}\rho^2\eta_{\mathrm{CSP}}\quad\forall t \quad (33)$$

$$P_{\mathrm{AD},s,t}=8(m_{\mathrm{AD},s,t})^3fL_{\mathrm{AD}}/D^5_{\mathrm{AD}}\rho^2\eta_{\mathrm{ADP}}\quad\forall t \quad (34)$$

$$P_{\mathrm{WF},s,t}=m_{\mathrm{WF},s,t}(h_{4,s}-h_{3,s})\quad\forall t \quad (35)$$

$$P_{\mathrm{C},s,t}=P_{\mathrm{WS},s,t}+P_{\mathrm{CS},s,t}+P_{\mathrm{AD},s,t}+P_{\mathrm{WF},s,t}\quad\forall t \quad (36)$$

$$-rd\le P_{\mathrm{e},s,t}-P_{\mathrm{e},s,t-1}\le ru\quad\forall t \quad (37)$$

$$\sum_{t=1}^{L^{\min}_{\mathrm{down}}}x_{s,t}=0 \quad (38)$$

$$\sum_{t'=t}^{t+T^{\min}_{\mathrm{down}}-1}(1-x_{s,t'})\ge T^{\min}_{\mathrm{down}}(x_{s,t-1}-x_{s,t}) \quad \forall t\in[L^{\min}_{\mathrm{down}}+1,N_{\mathrm{H}}-T^{\min}_{\mathrm{down}}+1] \quad (39)$$

$$\sum_{t'=t}^{N_{\mathrm{H}}}[1-x_{s,t'}-(x_{s,t-1}-x_{s,t})]\geq 0 \quad \forall t\in[N_{\mathrm{H}}-T_{\text{down}}^{\min}+2,N_{\mathrm{H}}] \tag{40}$$

$$\sum_{t=1}^{L_{\text{up}}^{\min}}(1-x_{s,t})=0 \tag{41}$$

$$\sum_{t'=t}^{t+T_{\text{up}}^{\min}-1} x_{s,t'}\geq T_{\text{up}}^{\min}y_{s,t} \quad \forall t\in[L_{\text{up}}^{\min}+1,N_{\mathrm{H}}-T_{\text{up}}^{\min}+1] \tag{42}$$

$$\sum_{t'=t}^{N_{\mathrm{H}}}(x_{s,t}-y_{s,t})\geq 0 \quad \forall t\in[N_{\mathrm{H}}-T_{\text{up}}^{\min}+2,N_{\mathrm{H}}] \tag{43}$$

where $x_{s,t}$ is the binary variable that is equal to 1 if SOTEC is on at time t, and 0 otherwise. Constraints (26)–(27) represent the correlations between binary $x_{s,t}$ and $y_{s,t}$. Constraints (29)–(36) are the thermodynamic model of SOTEC. $P_{\mathrm{C,\,s,\,t}}$ is the total energy consumption of four pumps in SOTEC. The ramp rate limits are presented in constraints (37) where rd and ru are the ramp-down limit and ramp-up limit of the generator unit in SOTEC. $T_{\text{down}}^{\min}$ and $T_{\text{up}}^{\min}$ are minimum-down time and maximum-up time of the generator unit in SOTEC. $L_{\text{down}}^{\min}$ and $L_{\text{up}}^{\min}$ are the length of time that SOTEC has to be down and to be up from the beginning of the planning horizon.

2) SPS Constraints

The capacity of SPS should be constrained due to the limited volume of the undersea reservoir. The fact that energy storing and releasing cannot be done simultaneously also has to be highlighted. Moreover, the maximum power of the turbine and pump are depicted as follows,

$$St_{s,1}=St_{\text{start}}+P_{\mathrm{pu},s,1}Ef_{\mathrm{pu}}-P_{\mathrm{tu},s,1}/Ef_{\mathrm{tu}} \tag{44}$$

$$St_{s,t}=St_{s,t-1}+P_{\mathrm{pu},s,t}\cdot Ef_{\mathrm{pu}}-P_{\mathrm{tu},s,t}/Ef_{\mathrm{tu}}\ \forall t\in[2,N_{\mathrm{H}}] \tag{45}$$

$$0\leq St_{s,t}\leq St_{\max}\quad\forall t \tag{46}$$

$$0\leq P_{\mathrm{tu},s,t}\leq P_{\mathrm{tu,max}}u_{s,t}\quad\forall t \tag{47}$$

$$0\leq P_{\mathrm{pu},s,t}\leq P_{\mathrm{pu,max}}v_{s,t}\quad\forall t \tag{48}$$

$$u_{s,t},v_{s,t}\in\{0,1\}\quad\forall t \tag{49}$$

$$u_{s,t}+v_{s,t}\leq 1\quad\forall t \tag{50}$$

$$a_{s,t}=\begin{cases}u_{s,1}\\ u_{s,t}-u_{s,t-1}\quad\forall t\in[2,N_{\mathrm{H}}]\end{cases} \tag{51}$$

$$b_{s,t}=\begin{cases}v_{s,1}\\ v_{s,t}-v_{s,t-1}\quad\forall t\in[2,N_{\mathrm{H}}]\end{cases} \tag{52}$$

$$z_{s,t}=\begin{cases}0 & (a_{s,t}=-1,0)\\ 1 & (a_{s,t}=1)\end{cases}\quad\forall t \tag{53}$$

$$l_{s,t}=\begin{cases}0 & (b_{s,t}=-1,0)\\ 1 & (b_{s,t}=1)\end{cases}\quad\forall t \tag{54}$$

where $u_{s,t}$ and $v_{s,t}$ are binary variables that are equal to 1 if the turbine and pump of SPS are on at the beginning of the time period, respectively, and 0 otherwise; $a_{s,t}$ and $b_{s,t}$ are variables that are equal to 1 if the turbine and pump of SPS start up at the time t, respectively, equal to -1 if shut down, and 0 otherwise.

3) Multi-Energy Balance and Other Constraints

$$P_{\mathrm{e},s,t}-P_{\mathrm{C},s,t}+P_{\mathrm{WP},s,t}+P_{\mathrm{TP},s,t}+g_{s,t}^{\mathrm{up}}+P_{\mathrm{tu},s,t}=G_{s,t}+g_{s,t}^{\mathrm{d}}+P_{\mathrm{pu},s,t}\quad\forall t \tag{55}$$

$$G_{1,t}=G_{2,t}=G_{3,t}\cdots=G_{N_{\mathrm{R}},t}\quad\forall t \tag{56}$$

Constraint (55) corresponds to the energy balancing constraint. Constraint (56) suggests that the electricity sold or purchased at time t in the day-ahead market is only relevant to the given market price irrespective of OWPP and TPP outputs, which also models the fact that there is only one offering curve submitted to the day-ahead market.

B. Real-time Optimization of the VPP Dispatch

In the real-time stage, the operator should make real-time scheduling decisions of SOTEC and SPS per hour after the realization of the OWPP output, solar radiation and TPP output, and then determine the strategy in the balancing market to regulate energy deviations. Therefore, the rolling horizon optimization is utilized for real-time dispatching in the second stage. During the optimization routine, every scheduling strategy is obtained by optimizing for the present dispatch cycle and taking into account the remaining dispatch cycles while looking ahead to the uncertainties of OWPP outputs, solar radiations and TTP outputs in future horizons. The objective function of the scenario-based rolling horizon optimization model in the second stage aims to minimize the real-time scheduling cost, including the cost of purchasing or selling electricity in the balancing market and star-up cost of SOTEC and SPS, plus the scheduling cost of all remaining future scenarios,

$$\begin{aligned}\min\ & \lambda_{t_0}\left(g_{t_0}^{\mathrm{up}}\varphi_{\mathrm{up}}-g_{t_0}^{\mathrm{d}}\varphi_{\mathrm{d}}\right)+y_{t_0}F_{\mathrm{o}}+z_{t_0}F_{\mathrm{tu}}+l_{t_0}F_{\mathrm{pu}}\\ &+\sum_{s=1}^{N_{\mathrm{R}}}\pi_{\mathrm{s}}\sum_{t=t_0+1}^{N_{\mathrm{H}}}\left[\lambda_{s,t}\left(g_{s,t}^{\mathrm{up}}\varphi_{\mathrm{up}}-g_{s,t}^{\mathrm{d}}\varphi_{\mathrm{d}}\right)+y_{s,t}F_{\mathrm{o}}\right.\\ &\left.+z_{s,t}F_{\mathrm{tu}}+l_{s,t}F_{\mathrm{pu}}\right]\end{aligned} \tag{57}$$

where λ_{t_0} and λ_{t} are the day-ahead market prices at present time t_0 and time t, respectively; $g_{t_0}^{\mathrm{up}}$ and $g_{s,t}^{\mathrm{up}}$ are the amount of electricity purchased at present time t_0 and time t under scenario s in the balancing market, respectively; $g_{t_0}^{\mathrm{d}}$ and $g_{s,t}^{\mathrm{d}}$ are the amount of electricity sold at present time t_0 and time t under scenario s in the balancing market, respectively; y_{t_0} and $y_{s,t}$ are binary variables that are equal to 1 if SOTEC starts up at time t_0 and time t in scenario s, respectively, and 0 otherwise; $z_{s,t}$ and $l_{s,t}$ are binary variables that are equal to 1 if the turbine and pump of SPS start up at the beginning of the current time t_0 and time t in scenario s, respectively, and equal to 0 otherwise.

The system constraints (26)–(54) can be applied to the real-time scheduling model as well. It's worth noting that the day-ahead market price $\lambda_{s,t}$ and electricity purchased or sold in the day-ahead market $G_{s,t}$ shall be constant in the real-time dispatch. Furthermore, the energy balance constraint at current time t_0 and time t in scenario s is expressed as follows,

$$P_{\mathrm{e},t_0} - P_{\mathrm{C},t_0} + P_{\mathrm{WP},t_0} + P_{\mathrm{TP},t_0} + g_{t_0}^{\mathrm{up}} + P_{\mathrm{tu},t_0} \quad (58)$$

$$= G_{t_0} + g_{t_0}^{\mathrm{d}} + P_{\mathrm{pu},t_0} \quad (59)$$

$$P_{\mathrm{e},s,t} - P_{\mathrm{C},s,t} + P_{\mathrm{WP},s,t} + P_{\mathrm{TP},s,t} + g_{s,t}^{\mathrm{up}} + P_{\mathrm{tu},s,t}$$

$$= G_{s,t} + g_{s,t}^{\mathrm{d}} + P_{\mathrm{pu},s,t} \quad \forall t \in [t_0+1, N_{\mathrm{H}}], \forall s \quad (60)$$

The flowchart of the developed optimal two-stage VPP scheduling model is depicted in Fig. 6. It's worth noting that the possible scenarios of renewable ocean energy outputs and electricity market prices from the time period $t_0 + 1$ to N_{H} should be updated by the timely forecasting scenarios in every scheduling cycle and the operator of the VPP only operates according to the obtained scheduling strategy in the present time t_0.

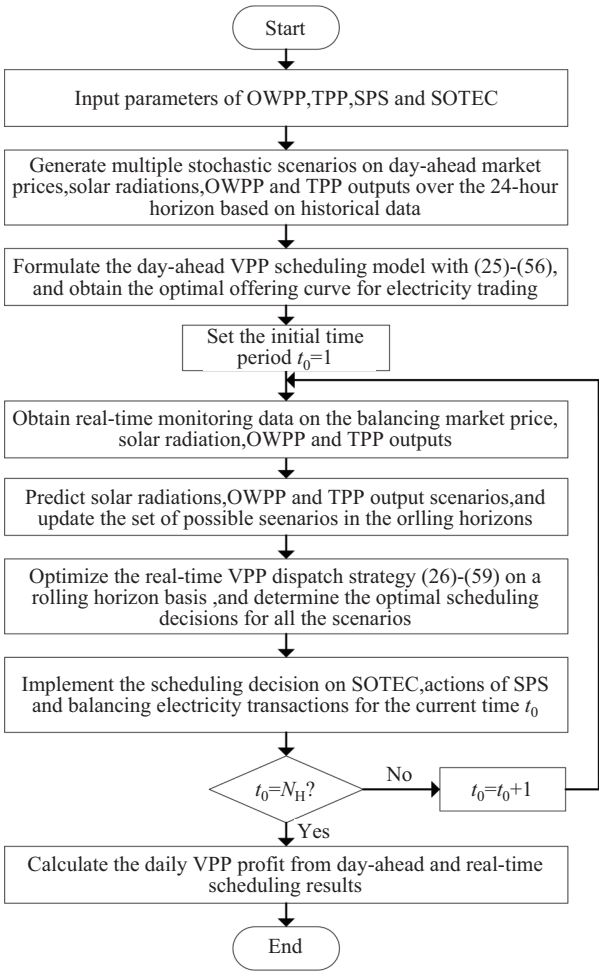

Fig. 6. Flowchart of the two-stage VPP dispatch model.

IV. Case Studies

A. System Description

The two-stage scheduling strategy is presented over one day with 24-time slots. The characteristics of SOTEC and TPP with SPS are shown in Tables I and II, respectively. A 10-block piecewise linear function is utilized to approximate the cubic function of the SOTEC pumps' energy consumption. It is assumed that SOTEC has been shut down for one hour before the considered time horizon.

TABLE I
Characteristics of SOTEC

Parameters		Symbol	Value
Warm seawater pipe	Length (m)	L_{WS}	50
	Diameter (m)	D_{WS}	8.9
Cold seawater pipe	Length (m)	L_{CS}	1000
	Diameter (m)	D_{CS}	7.9
Warm seawater temperature at depth 0 m (°C)		T_{WSI}	25.2
Cold seawater temperature at depth 1000 m (°C)		T_{CSI}	4.7
Friction factor of pipe		f	0.25
Turbine efficiency		η_{tur}	0.8
Generator efficiency		η_{gen}	0.9
Seawater pump efficiency		η_{WSP} η_{CSP} η_{ADP}	0.8
Working fluid pump efficiency		η_{WFP}	0.75
Solar collector area (m^2)		A_{sc}	6278
Heat transfer plate thickness (m)		δ_{P}	0.001
Heat transfer thermal conductivity (W/(m·K))		λ_{P}	160
Fouling resistances on the working fluid side (m^2·K/W)		R_{WF}	0.000007
Fouling resistances on the seawater side (m^2·K/W)		R_{S}	0.000017
Overall heat transfer coefficient of the evaporator (kW/m^2 K)		K_{E}	3.98
Overall heat transfer coefficient of the condenser (kW/m^2 K)		K_{C}	3.24
Heat transfer area of the evaporator (m^2)		A_{E}	6615
Heat transfer area of the condenser (m^2)		A_{C}	9346
Efficiency of the evaporator		η_{E}	0.7
Efficiency of the condenser		η_{C}	0.85

The VPP is aggregated by an OWPP with a capacity of 10 MW, a TPP with a capacity of 15 MW and a SOTEC plant with a capacity of 10 MW. The data of the wind speed and solar radiation are obtained from the software Meteonorm 7.3 and the height of the sea level is based on historical data [40]. The day-ahead market price data are extracted from APX Power UK [41]. In the day-ahead stage, the two-stage coordinated scheduling model characterizes the uncertainties of the electricity market prices, solar radiations, OWPP and TPP outputs by the initial stochastic scenarios of 10,000, and then the scenario reduction technique [42] is utilized to decrease the number of scenarios to 625 so as to lower the scale and computation time of the stochastic optimization while retaining a good approximation of system uncertainties. The five day-ahead market price scenarios of the reduced scenarios set are shown in Fig. 7. The overall two-stage scheduling strategy in (25)–(59) is a mixed-integer linear programming problem that can be solved utilizing CPLEX 12.8 on a personal computer with 2.8-GHz Intel Core i5 CPU and 16 GB RAM.

B. Comparative Results and Analysis

For further research, the following three comparative schemes are performed to verify the superiority of the developed system: 1) Scheme 1 implements the proposed two-stage coordinated scheduling model in Section III; 2) Scheme 2 adopts the conventional OTEC without the solar enhancement; 3) Scheme 3 implements the traditional TPP without SPS.

In the day-ahead stage, Fig. 8 illustrates the day-ahead hourly profit and cumulative profit in schemes 1–3. It's obvious that the hourly profit curve in the three schemes is basically consistent with the fluctuation in the market price curves. In hour 18, the peak profit happens which results from the peak

TABLE II
CHARACTERISTICS OF TPP WITH SPS

Parameters	Symbol	Value
Capacity of TPP (MW)	$P_{\mathrm{TP,max}}$	15
Charge capacity of SPS (MW·h)	$St_{\max}$	20
Located ocean depth of SPS (m)	H_{s}	30
Average hydraulic pressure of SPS (kPa)	P_{s}	302.82
Maximum power of the hydraulic reversible pump-turbines (MW)	$P_{\mathrm{tu,max}}$ $P_{\mathrm{pu,max}}$	5
Hydraulic reversible pump-turbine efficiency	Ef_{tur} Ef_{pu}	0.85
Inner volume of the subsea reservoir (m^3)	V_{s}	13592

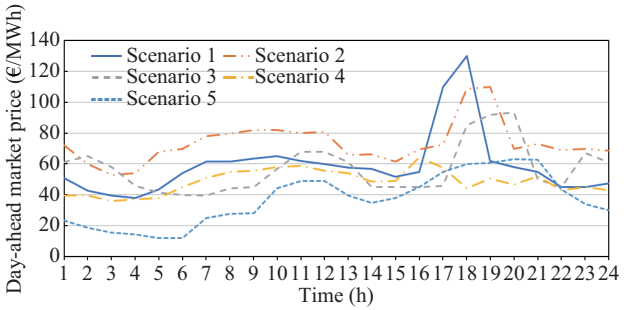

Fig. 7. Day-ahead market price scenarios.

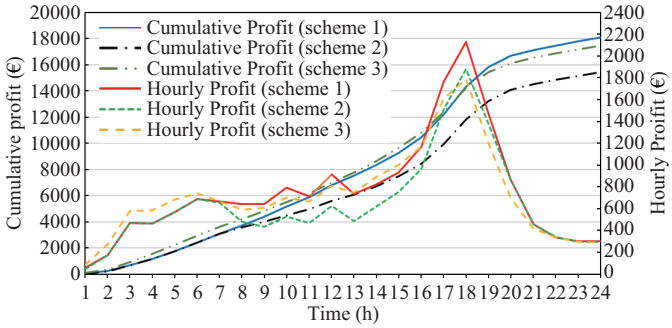

Fig. 8. Expected hourly and cumulative profit of VPP in schemes 1–3.

market price in the market price scenarios. It also can be found that the hourly profit in scheme 1 is always higher compared with scheme 2 due to the higher efficiency of SOTEC. The total daily profit under scheme 1 is Euro 18,072.60, which is 17.07% higher than Euro 1,5437.15 in scheme 2. Moreover, owing to the flexibility of SPS, the overall expected profit in scheme 1 is 3.54% higher than Euro 17,454.26 in scheme 3. Therefore, the comparative results demonstrate that VPP can achieve the arbitrage by the integration of TPP with SPS. Considering that if it implements the expected-value strategy, the profit is Euro 16,592.54. Therefore, the value of the stochastic solution (VSS) is Euro 1,480.06, which is 8.92% in relative terms.

As shown in Fig. 9, the efficiency of SOTEC in scheme 1 increases related to solar radiation. When the solar radiation is highest in hour 13, the efficiency of SOTEC in scheme 1 is more than twice as large as that in scheme 2. Fig. 10 shows the amount of electricity sold in the day-ahead transactions considering various renewable ocean energy and market price scenarios. It's obvious that the VPP sells more electricity to the day-ahead market during hours 6–20 in scheme 1 than that

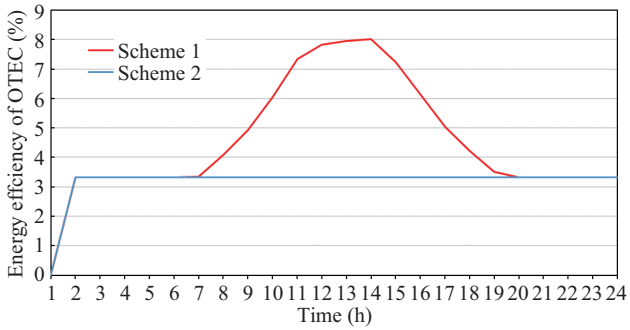

Fig. 9. Energy efficiency of OTEC in schemes 1 and 2.

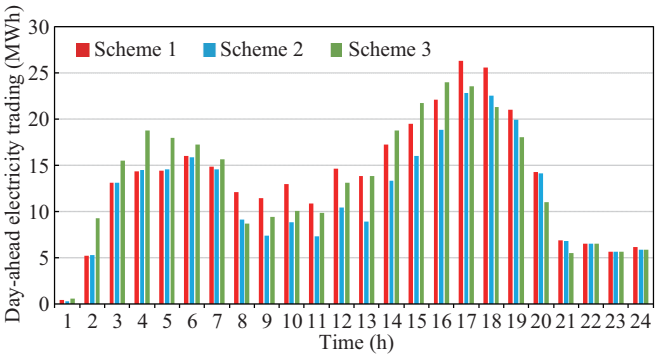

Fig. 10. Day-ahead offering strategy of VPP in schemes 1–3.

in scheme 2 due to the higher efficiency of SOTEC. When the electricity market price is low, VPP in schemes 1 and 2 tends to store the generated electricity rather than sell all generated electricity in scheme 3 during hours 2–7. Therefore, the amount of day-ahead trading electricity in scheme 3 is higher than that in schemes 1 and 2 during hours 2–7. On the contrary, SPS in schemes 1 and 2 tends to release energy when the electricity market price is high, which contributes to the higher amount of day-ahead trading electricity in schemes 1 and 2 than that in scheme 3 during hours 18–21. Because of the flexibility of SPS, the VPP tends to purchase electricity through the balancing market at a lower market price and sell electricity at a higher market price, which results in a higher total amount of electricity in scheme 1 than that in scheme 3.

As shown in Figs. 11–12, for the sake of clarity, assuming that the value in Fig. 11 is negative when SPS stores energy and the value in Fig. 12 is negative when the electricity is sold in the balancing market. Moreover, OWPP, TPP, and SOTEC outputs remain positive.

In the real-time stage, the amount of charging/discharging energy in SPS under schemes 1 and 2 is presented in Fig. 11. It can be found that the VPP tends to utilize the pumps of SPS to store the energy generated by the VPP or purchased from the market during hours 3–8, which results from the low day-ahead market price. On the contrary, the seawater is not pumped out of the subsea reservoir anymore since the electricity market price begins to rise in hour 16. Fig. 12 depicts the amount of electricity sold or purchased under schemes 1–3 in the balancing market. Table III gives the quantitatively comparative scheduling results for schemes 1–3. It can be found that the VPP tends to purchase electricity in

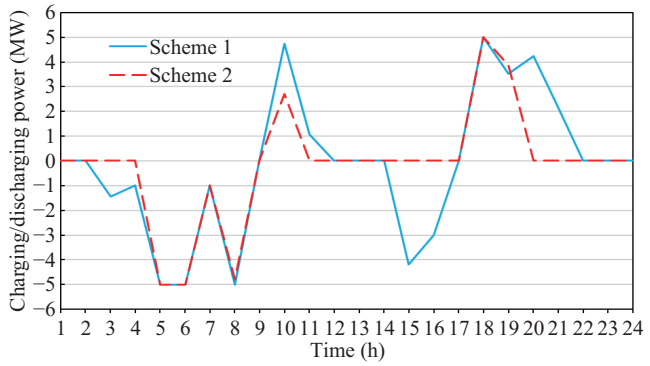

Fig. 11. Real-time operations of SPS.

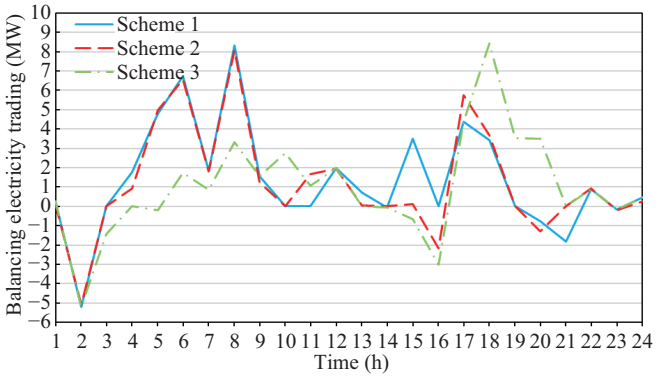

Fig. 12. Electricity transactions in the balancing market under schemes 1–3.

TABLE III
STATISTICAL SCHEDULING RESULTS IN SCHEMES 1–3

Scheme	1	2	3
Day-ahead profit (€)	**18808.82**	16356.62	18237.67
Balancing electricity sold (MW·h)	8.03	10.24	**10.74**
Balancing electricity purchased (MW·h)	**40.71**	38.66	36.58
Balancing market cost (€)	2066.41	1924.54	**2678.82**
Start-up cost (€)	234.32	234.32	**78.56**
Real-time operation cost (€)	2300.73	2158.86	**2757.38**
Final profit (€)	**16508.09**	14197.76	15480.29

schemes 1 and 2 as a consequence of the low electricity market price during hours 4–9. In addition, the VPP also purchases electricity at a higher electricity market price during hours 17–18, which results from the limited output of SPS and fluctuations of renewable ocean energy. Moreover, due to the lack of SPS and fluctuations of renewable ocean energy in hours 18–21, the VPP in scheme 3 has to buy more electricity in the balancing market compared to schemes 1 and 2 when the market price is high. Therefore, the balancing transaction cost in scheme 3 is 29.64% higher than that in scheme 1 despite the amount of electricity purchased in scheme 3 is lower than that in scheme 1.

C. Discussion

The initial scenario tree is generated on the basis of forecasting results from historical data. For the purpose of capturing the forecasting uncertainties, Monte Carlo simulations are utilized for generating scenarios by sampling from Gaussian probability distributions of renewable ocean energy output and day-ahead market price forecasting errors. Moreover, the scenario reduction technique is implemented for removing similar scenarios while reserving the characteristics of the initial scenarios. The comparative studies on stochastic scenarios of various scales have been further implemented to research the scale of the initial scenarios and reduced scenarios in the day-ahead scheduling model. The daily profit of the VPP and simulation time with different numbers of initial scenarios and reduced scenarios in the day-ahead stage are shown in Tables IV and V, respectively. The results indicate that the daily profit of the VPP would be promoted with the increased number of original scenarios and reduced scenarios. However, the computing time would rapidly increase. Comparing the results of the reduced scenarios on the same scale, it can be found that the simulations in more than 10,000 original scenarios have approximate profits. Similarly, with the 10,000 original scenarios, the simulations in more than 625 reduced scenarios have approximate profits while the computing time increases rapidly. Therefore, the two-stage coordinated day-ahead scheduling stage characterizes the uncertainties in the electricity market prices, solar radiations, OWPP and TPP outputs using the initial stochastic scenarios of 10,000 based on historical data, and then the scenario reduction technique is utilized to decrease the number of scenarios into 625 so as to lower the scale and computation time of the stochastic optimization while retaining a good approximation of system uncertainties.

TABLE IV
DAILY PROFITS IN DIFFERENT NUMBERS OF DAY-AHEAD SCENARIOS (€)

#of initial scenarios	#of reduced scenarios				
	100	400	625	800	1000
500	17095.19	17496.37	17731.14	17804.19	17794.92
2500	17288.63	17673.53	17928.25	17988.53	17996.17
5000	17372.34	17749.59	18009.81	18075.17	18087.42
10000	17431.54	17803.61	**18072.60**	18130.73	18149.36
15000	17462.78	17836.48	18109.87	18159.82	18181.17
20000	17477.13	17852.42	18126.19	18173.94	18200.75
25000	17485.93	17859.34	18137.69	18180.67	18205.74

TABLE V
SIMULATION TIME IN DIFFERENT NUMBERS OF DAY-AHEAD SCENARIOS (MIN)

#of initial scenarios	#of reduced scenarios				
	100	400	625	800	1000
500	3.72	6.35	8.26	9.43	12.79
2500	4.94	7.28	9.54	11.75	15.41
5000	6.15	9.64	11.13	13.92	18.35
10000	9.23	12.41	**14.61**	17.45	23.87
15000	15.34	18.26	20.72	22.16	28.12
20000	23.82	25.79	27.41	31.26	37.49
25000	34.15	36.32	37.83	42.47	49.37

In order to investigate the scalability and real-time applicability of the two-stage coordinated scheduling model, the daily profit of the VPP and simulation time with different numbers of initial scenarios and reduced scenarios in the real-time stage are shown in Tables VI and VII, respectively. It can be found from Table VI that, comparing the results of the reduced scenarios in the same scale, the simulations in more than

TABLE VI
DAILY PROFITS IN DIFFERENT NUMBERS OF REAL-TIME SCENARIOS (€)

#of initial scenarios	#of reduced scenarios				
	5	10	20	30	50
500	15965.24	16158.72	16266.48	16311.27	16338.52
1000	16103.93	16301.13	16405.16	16446.41	16469.81
2000	16240.72	16419.68	16515.49	16547.15	16563.61
4000	16326.47	**16508.09**	16607.85	16644.29	16663.75
6000	16364.85	16551.18	16643.12	16674.19	16689.24
8000	16388.96	16580.87	16671.26	16703.84	16716.98
10000	16409.14	16592.39	16680.77	16719.52	16732.37

TABLE VII
SIMULATION TIME IN DIFFERENT NUMBERS OF REAL-TIME SCENARIOS (S)

#of initial scenarios	#of reduced scenarios				
	5	10	20	30	50
500	28.96	46.89	89.25	199.43	267.41
1000	31.14	50.06	93.54	204.84	273.89
2000	33.52	53.16	97.42	207.41	276.15
4000	37.69	**58.74**	99.93	212.36	281.26
6000	39.41	60.94	103.28	215.76	286.51
8000	46.59	62.94	107.84	220.13	294.41
10000	52.16	65.41	110.63	224.36	308.18

4,000 original scenarios have approximate profits. Moreover, with the number of reduced scenarios of more than 10, the simulation time is more than one minute, which is not suitable for real-time VPP dispatching. Therefore, taking both the daily VPP profit and real-time applicability into consideration, 4,000 initial scenarios and 10 reduced scenarios is a trade-off decision to satisfy the requirement on the response speed of the real-time electricity market at the minute level [43]. The computing time of the rolling optimization in the second stage of scheduling is 58.74 seconds.

V. CONCLUSION

This paper proposes an optimal scheduling model for coordinating various renewable ocean energy to flexibly participate in the electricity market. The findings of this paper are concluded as follows: 1) The combination of solar energy and the closed-cycle OTEC was found to effectively promote the efficiency of OTEC, which contributes to a 17.07% higher expected profit in the market transaction; 2) The activities of SPS are basically consistent with the fluctuation of the day-ahead market price curve. Therefore, with the coordinated tidal-storage operation model, the VPP can make the arbitrage to obtain a 3.54% higher profit; 3) Comparative studies and the VSS, which is 8.92% of the profit under the expected-value strategy, demonstrate the superior performance of the proposed methodology to maximize the short-term expected profit under uncertainties of renewable ocean energy and electricity market prices.

REFERENCES

[1] T. Wilberforce, Z. El Hassan, A. Durrant, J. Thompson, B. Soudan, and A. G. Olabi, "Overview of ocean power technology," *Energy*, vol. 175, pp. 165–181, May 2019.

[2] M. Melikoglu, "Current status and future of ocean energy sources: a global review," *Ocean Engineering*, vol. 148, pp. 563–573, Jan. 2018.

[3] X. P. Zhang and P. L. Zeng, "Marine energy technology [Sanning the Issue]," *Proceedings of the IEEE*, vol. 101, no. 4, pp. 862–865, Apr. 2013.

[4] Global Wind Report, Brussels, Belgium, Global Wind Energy Council 2019, https://gwec.net/global-wind-report-2019.

[5] A. von Jouanne and T. K. A. Brekken, "Ocean and geothermal energy systems," *Proceedings of the IEEE*, vol. 105, no. 11, pp. 2147–2165, Nov. 2017.

[6] R. Z. Lu, T. Ding, B. Y. Qin, J. Ma, X. Fang, and Z. Y. Dong, "Multi-Stage stochastic programming to joint economic dispatch for energy and reserve with uncertain renewable energy," *IEEE Transactions on Sustainable Energy*, vol. 11, no. 3, pp. 1140–1151, Jul. 2020.

[7] T. Das, R. Roy, and K. K. Mandal, "Impact of the penetration of distributed generation on optimal reactive power dispatch," *Protection and Control of Modern Power Systems*, vol. 5, no. 1, pp. 31, Dec. 2020.

[8] M. Faizal and M. R. Ahmed, "Experimental studies on a closed cycle demonstration OTEC plant working on small temperature difference," *Renewable Energy*, vol. 51, pp. 234–240, Mar. 2013.

[9] C. Bernardoni, M. Binotti, and A. Giostri, "Techno-economic analysis of closed OTEC cycles for power generation," *Renewable Energy*, vol. 132, pp. 1018–1033, Mar. 2019.

[10] S. M. Nosratabadi, R. A. Hooshmand, and E. Gholipour, "A comprehensive review on microgrid and virtual power plant concepts employed for distributed energy resources scheduling in power systems," *Renewable and Sustainable Energy Reviews*, vol. 67, pp. 341–363, Jan. 2017.

[11] P. Hou, W. H. Hu, M. Soltani, and Z. Chen, "Optimized placement of wind turbines in large-scale offshore wind farm using particle swarm optimization algorithm," *IEEE Transactions on Sustainable Energy*, vol. 6, no. 4, pp. 1272–1282, Oct. 2015.

[12] P. Hou, W. H. Hu, M. Soltani, C. Chen, B. H. Zhang, and Z. Chen, "Offshore wind farm layout design considering optimized power dispatch strategy," *IEEE Transactions on Sustainable Energy*, vol. 8, no. 2, pp. 638–647, Apr. 2017.

[13] H. Yuan, N. Mei, and P. L. Zhou, "Performance analysis of an absorption power cycle for ocean thermal energy conversion," *Energy Conversion and Management*, vol. 87, pp. 199–207, Nov. 2014.

[14] M. H. Yang and R. H. Yeh, "Analysis of optimization in an OTEC plant using organic Rankine cycle," *Renewable Energy*, vol. 68, pp. 25–34, Aug. 2014.

[15] L. Xiao, S. Y. Wu, T. T. Yi, C. Liu, and Y. R. Li, "Multi-objective optimization of evaporation and condensation temperatures for subcritical organic Rankine cycle," *Energy*, vol. 83, pp. 723–733, Apr. 2015.

[16] A. Angeloudis, S. C. Kramer, A. Avdis, and M. D. Piggott, "Optimising tidal range power plant operation," *Applied Energy*, vol. 212, pp. 680–690, Feb. 2018.

[17] J. Q. Xia, R. A. Falconer, and B. L. Lin, "Impact of different operating modes for a Severn Barrage on the tidal power and flood inundation in the Severn Estuary, UK," *Applied Energy*, vol. 87, no. 7, pp. 2374–2391, Jul. 2010.

[18] F. Yilmaz, "Energy, exergy and economic analyses of a novel hybrid ocean thermal energy conversion system for clean power production," *Energy Conversion and Management*, vol. 196, pp. 557–566, Sept. 2019.

[19] H. Aydin, H. S. Lee, H. J. Kim, S. K. Shin, and K. Park, "Off-design performance analysis of a closed-cycle ocean thermal energy conversion system with solar thermal preheating and superheating," *Renewable Energy*, vol. 72, pp. 154–163, Dec. 2014.

[20] Y. Kuang, X. L. Wang, H. Y. Zhao, T. Qian, J. X. Wang, and X. F. Wang, "Model-free demand response scheduling strategy for virtual power plant considering risk attitude of consumer," *CSEE Journal of Power and Energy Systems*, Early Access, DOI: 10.17775/CSEEJPES.2020.03120, 2021.

[21] H. J. Gao, F. Zhang, Y. M. Xiang, S. Y. Ye, X. Liu, and J. Y. Liu, "Bounded rationality based multi-VPP trading in local energy market: A dynamic game approach with different trading targets," *CSEE Journal of Power and Energy Systems*, doi: 10.17775/CSEEJPES.2021.01600.

[22] H. Pandžić, J. M. Morales, A. J. Conejo, and I. Kuzle, "Offering model for a virtual power plant based on stochastic programming," *Applied Energy*, vol. 105, pp. 282–292, May 2013.

[23] B. Zhou, X. Liu, Y. J. Cao, C. B. Li, C. Y. Chung, and K. W. Chan, "Optimal scheduling of virtual power plant with battery degradation cost," *IET Generation, Transmission & Distribution*, vol. 10, no. 3, pp. 712–725, Feb. 2016.

[24] E. G. Kardakos, C. K. Simoglou, and A. G. Bakirtzis, "Optimal offering strategy of a virtual power plant: a stochastic bi-level approach," *IEEE Transactions on Smart Grid*, vol. 7, no. 2, pp. 794–806, Mar. 2016.
[25] M. Shabanzadeh, M. K. Sheikh-El-Eslami, and M. R. Haghifam, "The design of a risk-hedging tool for virtual power plants via robust optimization approach," *Applied Energy*, vol. 155, pp. 766–777, Oct. 2015.
[26] M. Rahimiyan and L. Baringo, "Strategic bidding for a virtual power plant in the day-ahead and real-time markets: a price-taker robust optimization approach," *IEEE Transactions on Power Systems*, vol. 31, no. 4, pp. 2676–2687, Jul. 2016.
[27] B. Zhou, K. Zhang, K. W. Chan, C. B. Li, X. Lu, S. Q. Bu, and X. Gao, "Optimal coordination of electric vehicles for virtual power plants with dynamic communication spectrum allocation," *IEEE Transactions on Industrial Informatics*, vol. 17, no. 1, pp. 450–462, Jan. 2021.
[28] D. C. Yang, S. W. He, Q. Y. Chen, D. Q. Li, H. Pandžić, "Bidding strategy of a virtual power plant considering carbon-electricity trading," *CSEE Journal of Power and Energy Systems*, vol. 5, no. 3, pp. 306–314, Sept. 2019.
[29] M. Vasirani, R. Kota, R. L. G. Cavalcante, S. Ossowski, and N. R. Jennings, "An agent-based approach to virtual power plants of wind power generators and electric vehicles," *IEEE Transactions on Smart Grid*, vol. 4, no. 3, pp. 1314–1322, Sept. 2013.
[30] L. Wang and C. B. Huang, "Dynamic stability analysis of a grid-connected solar-concentrated ocean thermal energy conversion system," *IEEE Transactions on Sustainable Energy*, vol. 1, no. 1, pp. 10–18, Apr. 2010.
[31] E. W. Lemmon, M. L. Huber, and M. O. McLinden, "NIST reference fluid thermodynamic and transport properties-Refprop: version 9.0," National Institute of Standards and Technology, Gaithersburg, Maryland, 2010.
[32] R. Soto and J. Vergara, "Thermal power plant efficiency enhancement with ocean thermal energy conversion," *Applied Thermal Engineering*, vol. 62, no. 1, pp. 105–112, Jan. 2014.
[33] H. Lee, Y. Hwang, and R. Radermacher, "Analytical investigation of low temperature lift energy conversion systems with renewable energy source," *Applied Thermal Engineering*, vol. 68, no. 1–2, pp. 92–99, Jul. 2014.
[34] Z. X. Wu, H. J. Feng, L. G. Chen, W. Tang, J. C. Shi, and Y. L. Ge, "Constructal thermodynamic optimization for ocean thermal energy conversion system with dual-pressure organic Rankine cycle," *Energy Conversion and Management*, vol. 210, pp. 112727, Apr. 2020.
[35] S. Farahat, F. Sarhaddi, and H. Ajam, "Exergetic optimization of flat plate solar collectors," *Renewable Energy*, vol. 34, no. 4, pp. 1169–1174, Apr. 2009.
[36] A. H. Slocum, G. E. Fennell, G. Dundar, B. G. Hodder, J. D. C. Meredith, and M. A. Sager, "Ocean renewable energy storage (ORES) system: analysis of an undersea energy storage concept," *Proceedings of the IEEE*, vol. 101, no. 4, pp. 906–924, Apr. 2013.
[37] R. Loisel, M. Sanchez-Angulo, F. Schoefs, and A. Gaillard, "Integration of tidal range energy with undersea pumped storage," *Renewable Energy*, vol. 126, pp. 38–48, Oct. 2018.
[38] T. Ding, Y. Hu, and Z. H. Bie, "Multi-stage stochastic programming with nonanticipativity constraints for expansion of combined power and natural gas systems," *IEEE Transactions on Power Systems*, vol. 33, no. 1, pp. 317–328, Jan. 2018.
[39] T. Ding, Q. R. Yang, X. Y. Liu, C. Huang, Y. H. Yang, M. Wang, and F. Blaabjerg, "Duality-free decomposition based data-driven stochastic security-constrained unit commitment," *IEEE Transactions on Sustainable Energy*, vol. 10, no. 1, pp. 82–93, Jan. 2019.
[40] National Marine Data Information Center [Online]. Available: https://www.cnss.com.cn/tide/.
[41] UKPX auction historical data [Online]. Available: http://www.apxgroup.com/market-results/apxpower-uk/ukpx-auction-historical-data/.
[42] J. Dupacova, N. Gröwe-Kuska, and W. Römisch, "Scenario reduction in stochastic programming," *Mathematical Programming*, vol. 95, no. 3, pp. 493–511, Mar. 2003.
[43] W. Pei, Y. Du, W. Deng, K. Sheng, H. Xiao, and H. Qu, "Optimal bidding strategy and intramarket mechanism of microgrid aggregator in real-time balancing market," *IEEE Transactions on Industrial Informatics*, vol. 12, no. 2, pp. 587–596, Apr. 2016.

Siyuan Guo received a B.Sc. degree in Electrical Engineering from Zhengzhou University, Zhengzhou, China, in 2019. He is currently pursuing a Ph.D. degree at the College of Electrical and Information Engineering in Hunan University, Changsha, China. His major research interests include renewable energy generation and resilience-oriented planning and operation.

Bin Zhou (S'11–M'13–SM'17) received the B.Sc. degree in Electrical Engineering from Zhengzhou University, Zhengzhou, China, in 2006, the M.S. degree in Electrical Engineering from South China University of Technology, Guangzhou, China, in 2009, and the Ph.D. degree in Electrical Engineering from The Hong Kong Polytechnic University, Hong Kong, China, in 2013. Afterwards, he worked as a Research Associate and subsequently a Postdoctoral Fellow in the Department of Electrical Engineering of The Hong Kong Polytechnic University. Now, he is an Associate Professor in the College of Electrical and Information Engineering, Hunan University, Changsha, China. His main fields of research include resilience-oriented power system planning and operation, multi-energy network modelling, analytics and assessment.

Ka Wing Chan (M'98) received B.Sc. (with First Class Honors) and Ph.D. degrees in Electronic and Electrical Engineering from the University of Bath, Bath, U.K., in 1988 and 1992, respectively. He currently is an Associate Head and Associate Professor in the Department of Electrical Engineering of The Hong Polytechnic University. His general research interests include smart grid and renewable energy, power system stability analysis and control, power system planning and optimization, real-time power system simulation.

Siqi Bu (S'11–M'12–SM'17) received a Ph.D. degree in Electric Power and Energy Research Cluster from the Queen's University of Belfast, Belfast, U.K., in 2012, where he continued his postdoctoral research work before entering industry. He was with National Grid U.K. as an Experienced U.K. National Transmission System Planner and Operator. He is currently an Assistant Professor with The Hong Kong Polytechnic University, Hong Kong, and a Chartered Engineer with the U.K. Royal Engineering Council, London, U.K. His research interests include power system stability analysis and operation control, including wind power generation, PEV, HVDC, FACTS, ESS, and VSG.

Canbing Li (M'06–SM'13) received B.E. and Ph.D. degrees in Electrical Engineering from Tsinghua University, Beijing, China, in 2001 and 2006, respectively. He is currently with the School of Electronic Information and Electrical Engineering, Shanghai Jiao Tong University. His current research interests include power systems, smart grid, renew able energy, with an emphasis on large-scale power system dispatch, economic and secure operation of power systems, energy efficiency and energy saving in smart grids, electric demand management of data centers, and vehicle-to-grid technologies.

Nian Liu (S'06–M'11) received B.S. and M.S. degrees in Electric Engineering from Xiangtan University, Hunan, China, in 2003 and 2006, respectively, and a Ph.D. degree in Electrical Engineering from North China Electric Power University, Beijing, China, in 2009. He is a Professor with the School of Electrical and Electronic Engineering at North China Electric Power University. He is a member of the State Key Laboratory of Alternate Electrical Power System with Renewable Energy Sources and a member of the Standardization Committee of Power Supply and Consumption in the Power Industry of China. He was a Visiting Research Fellow at RMIT University, Melbourne, Australia, from 2015 to 2016. His major research interests include multi-energy system integration, microgrids, cyber-physical energy system and renewable energy integration. Dr. Liu has authored or co-authored more than 160 journal and conference publications and has been granted more than 10 patents of China. He is an Editor of IEEE Transactions on Smart Grid, IEEE Transactions on Sustainable Energy, IEEE Power Engineering Letters, and the Journal of Modern Power Systems and Clean Energy (MPCE).

Cong Zhang (M'18) received the Ph.D. degree in Mathematics from School of Mathematics in South China University of Tehnology, Guangzhou, China, in 2013. After that, he began to research electrical engineering, and now he is an Associate Professor with the College of Electrical and Information Engineering, Hunan University, Changsha, China. His current research interests include reactive power optimization incorporating uncertainties, interval power flow analysis.